Parameter selection in limited data cone-beam CT reconstruction using edge-preserving total variation algorithms

Manasavee Lohvithee, Ander Biguri, Manuchehr Soleimani

Engineering Tomography Lab (ETL), University of Bath, Bath, UK

E-mail: ml902@bath.ac.uk

Abstract.

There are a number of powerful total variation (TV) regularization methods with great promises in limited data cone-beam CT reconstruction with an enhancement of image quality. These promising TV methods require careful selection of image reconstruction parameters for which there is no well established criteria. This paper presents a comprehensive valuation of parameter selection in a number of major TV-based reconstruction algorithms. The appropriate way of selecting the values for each individual parameter has been suggested. Finally, the new adaptive-weighted projection-controlled steepest descent (AwPCSD) algorithm is presented which implements the edge-preserving function for CBCT reconstruction with limited data. The proposed algorithm shows significant robustness compared to other three existing algorithms: ASD-POCS, AwASD-POCS and PCSD. The proposed AwPCSD algorithm is able to preserve the edges of the reconstructed images better with less sensitive parameters to tune.

Keywords: Total variation (TV), Edge-preserving function, Parameter tuning, Computed tomography, Iterative reconstruction, Limited data reconstruction

1. Introduction

X-ray radiation has long been discovered by Wilhelm C. Roentgen [1] and followed by Hounsfield's invention of the x-ray tomographic scanner in 1972 [2]. Since then, the X-ray CT has been extensively used especially for clinical diagnosis. More recent X-ray CT is being adapted for treatment planning by image guided radiation therapy(IGRT) as it can provide a many dimension view of the organ or region of interest [3].

One major concern of the x-ray CT in medical analysis is the high radiation dose delivered to a patient during clinical exams. This is particularly true in the radiation therapy sessions where an x-ray cone-beam CT (CBCT) scan is needed at the beginning of each session to observe a patient's anatomical change in response to the treatments. It has been reported that a high radiation dose can increase lifetime risk of cancer in patients [3][4]. One method to reduce the radiation dose of x-ray CT imaging is to lower mAs levels in CT data acquisition process [7]. By doing this, number of X-ray photon impinging on detector bins will be insufficient, which results in a high level of quantum noise on the sinogram [10]. Another method is to reconstruct CT image from sparse-view projection data [5][6]. However, when the number of projection views is reduced, the reconstructed result obtained from a conventional filtered back-projection (FBP) suffers some artifacts because the number of projection views does not satisfy the Shannon sampling theorem [11].

Generally, there are two categories of methods for CBCT reconstruction: analytic inversion algorithms and iterative methods. The well-known Feldkamp, Davis and Kress (FDK) method [8] is commonly used in clinical CT scanners and advanced commercial cone-beam scanners [9]. This method lies in the first category and works efficiently and accurately if projection data are well sampled.

A problem with the FDK reconstruction method happens when an amount of projection data is insufficient. This problem commonly occurs due to physical constraints such as imaging hardware, scanning geometry and ionizing radiation exposure. In such circumstances, the FDK method performs less efficiently and suffers from artifacts [5] [12].

The iterative reconstruction methods produce good quality images when the projection data are not theoretically sufficient for exact image reconstruction [13],[14],[15]. A minimization problem of CT reconstruction can be performed using iterative algorithms by formulating the data-consistency constraint with additional regularization term. This term is used to select a unique solution out of the set of feasible solutions that agree with the available projection data.

Minimizing total variation (TV) norm of the image is widely used as a common approach for regularization. In [5], Sidky et al proposed TV minimization algorithm with constraints enforced by projection onto convex sets (TV-POCS) and then the adaptive-steepest-descent-POCS (ASD-POCS) in [12]. In their studies, a constrained TV minimization algorithm for image reconstruction in circular cone-beam CT is developed where image TV norm is the objective function to be minimized while data

fidelity is a constraint.

Despite the advantages of using image TV norm as a regularization term, over-smoothing in the reconstructed image is a main concern [16]. The TV-based approaches uniformly penalize the image gradient regardless of the image structures. As a result, edges of the reconstructed image tend to be frequently oversmoothed, which leads to the loss of low-contrast information [10].

Many existing research has tried to overcome the over-smoothing problem of TV regularization algorithm. Tian et al [10] proposed a TV-based edge preserving (EPTV) model to preserve more low-contrast structures and edges by introducing a penalty weight to every TV term. This penalty weight is formulated as an exponential function of the local image-intensity gradients and adaptively updated during the reconstruction process. However, only isotropic edge property was considered in the EPTV model. Later on, Liu et al [16] proposed an adaptive-weighted TV (AwTV-POCS) model in which the associated weights were also expressed as an exponential but considered the anisotropic edge property of an image. Better performance has been achieved in preserving edge details with the AwTV-POCS model.

Another drawback of TV regularization algorithms is the presence of an initial set of parameters in the minimization of the TV norm. The set of optimal parameters are difficult to select and can only be determined by considerable numbers of trials and errors ,which is a time-consuming and tedious process [17]. A number of researches have tried to overcome this drawback. Liu et al proposed a nonparametric method to automatically update TV regularization step-size according to the differences from POCS step in the projection domain (projection controlled steepest descent,PCSD) and image domain (image controlled steepest descent,ICSD) [18] [19]. These 2 algorithms: PCSD and ICSD require fewer parameters than ASD-POCS and achieve similar or better reconstruction images.

This paper proposes a new algorithm called "adaptive-weighted PCSD (AwPCSD)" algorithm, which is based on the PCSD algorithm proposed by Liu et al [19] with additional edge-preserving function as proposed by Liu et al [16]. By doing so, it is hopeful that this AwPCSD algorithm will be able to preserve the edges of the reconstructed image better with less initial parameters to set than ASD-POCS algorithm.

In addition, this work aims to analyse the sensitivity of initial parameters required for the TV regularization algorithms. These parameters play an important role for the reconstruction performance of the algorithms. It is useful to examine the sensitivity that the reconstruction image has to value change on these parameters, in order to know which ones to prioritize when tuning the algorithm. Ultimately, heuristics on how to choose this parameters are desired, to minimize or completely avoid rerunning the reconstruction with different parameters.

The sensitivity of all the parameters is analysed using two image quality metrics: Root mean squared error (RMSE) and Correlation coefficient (CC) for the proposed algorithm , AwPCSD, in comparison with other three existing algorithms: ASD-POCS,

AwTV-POCS and PCSD to evaluate the performance of the proposed algorithm. The data set used in this study is a digital XCAT phantom which contains thorax anatomy structures [20]. The number of projection used to reconstruct an image is chosen to be 20 views to also compare the performance of these 4 algorithms in limited data scenario.

The edge preserving property of the TV-based reconstruction algorithms is analysed by comparing the image profiles along the horizontal and vertical lines of the reconstructed images with the optimal set of parameters. In addition, the proposed algorithm is evaluated further using the real microCT datasets, the SophiaBeads Datasets [31].

The organization of the paper is as follows. In section 2, a CT image reconstruction problem and a TV minimization approach as well as an edge-preserving function and reconstruction algorithms are explained. The stopping criterion and parameters for TV regularization algorithms are described in section 3. Section 4 contains the results from the sensitivity analysis of each parameter and further analysis of edge-preserving property using 1D profiles plot. The experimental evaluation of the real microCT datasets is explained in section 5. Section 6 discusses and concludes the paper.

2. Methods

2.1. CT image reconstruction problem and TV minimization approach

In circular CBCT, an attenuation of photons being absorbed by an object of interest, $f(x)$, is provided by a set of line integrals [17]. Given that a rotation angle of an x-ray source is a, the cone-beam projection measured at a point (u, v) on a detector can be expressed as

$$p(u, v, a) = \int_0^\infty f(s(a) + \lambda\theta(a, u, v))d\lambda \tag{1}$$

where the source location s is defined as

$$s(a) = (Rcos\ a, Rsin\ a, 0) \tag{2}$$

where R is the distance between the source location and the centre of rotation, $\lambda \in [0, \sqrt{u^2 + v^2 + D^2}]$, D is the distance between source to detector, $\theta(a, u, v)$ is the ray direction vector indicating the direction of the ray from the source location $s(a)$ through the object to the point (u, v) on the detector.

The projection acquisition model in equation 1 can be approximated using a system of linear equations as

$$Ax = b + e \tag{3}$$

where x is a vector containing the x-ray linear attenuation coefficients of the image in lexicographical order, e is the additive noise associated with the measurement, A is a system matrix describing the intersections between each particular ray and the image

voxels. The vector b represents projection data measured on image detectors at various projection in lexicographical order.

In an ideal scenario, the image reconstruction problem is solved by finding x given a set of data b , in other words, inverting the system of linear equation 3. However, the system matrix A is ill-conditioned due to two main reasons: insufficient coverage in the scanning configuration or under-sampling set of projection data in the case of few-view CT scanning.

From equation 3, a minimization problem can be proposed as

$$x^* = argmin_x ||Ax - b||^2 + G(x) \tag{4}$$

where $G(x)$ is an optional term that describes a regularization function. This minimization problem can be solved using a wide range of iterative algorithms. In this study, we are interested in the minimization of image total variation (TV) norm, which can help to differentiate infinitely many solutions to equation 3 and obtain the solution with the desired image properties as the final reconstructed image [10]. The TV norm for three-dimensional cone beam CT projection is approximated using finite differences as following equation

$$G(x) = ||x||_{TV} = \sum_{ijk} \sqrt{(x_{ijk} - x_{ij-1k})^2 + (x_{ijk} - x_{i-1jk})^2 + (x_{ijk} - x_{ijk-1})^2} \tag{5}$$

where i, j, k are indices of image voxel in three dimensions.

2.2. Edge-preserving function

One disadvantage of implementing the TV regularization approach is the over-smoothing of the reconstructed image especially at the edges due to the assumption of piecewise constant distribution for the desired image [16]. The edges are significant structural information of the image. Hence, the edge preservation is a critical requirement in many clinical analysis especially in IGRT.

One way to address this problem is to use priors other than conventional TV to improve preservation of fine details. The TV-based edge preserving (EPTV) model was proposed by Tian et al [10] to bring in different weights in the TV term from edges and constant areas of the to-be-estimated image. However, only isotropic edge property was considered in this model.

The anisotropic edge property of an image is considered in the adaptive-weighted TV (AwTV) model proposed by Liu et al [16]. The adaptive-weighted TV norm of the to-be-reconstructed image in 3D case is defined as

$$||x||_{AwTV} = \sum_{ijk} \sqrt{w_{i,i-1,j,j,k,k}(x_{ijk} - x_{i-1jk})^2 + w_{i,i,j,j,k,k-1}(x_{ijk} - x_{ijk-1})^2} \\ \sqrt{+w_{i,i,j,j-1,k,k}(x_{ijk} - x_{ij-1k})^2} \tag{6}$$

$$w_{i,i-1,j,j,k,k} = exp\left[-\left(\frac{x_{ijk} - x_{i-1jk}}{\delta}\right)^2\right] \tag{7}$$

$$w_{i,i,j,j,k,k-1} = exp\left[-\left(\frac{x_{ijk} - x_{ijk-1}}{\delta}\right)^2\right] \tag{8}$$

$$w_{i,i,j,j-1,k,k} = exp\left[-\left(\frac{x_{ijk} - x_{ij-1k}}{\delta}\right)^2\right] \tag{9}$$

where δ is a scale factor controlling the amount of smoothing being applied to the image voxel at edges relative to non-edge region during each iteration.

This pattern of weight choosing is based on the works proposed by Perona and Malik [29] and Wang et al [30]. An anisotropic penalty term is defined using the intensity difference between neighbouring pixels. By doing so, it is possible to take the change of local voxel intensities into consideration.

For a smaller change of local voxel intensities, a stronger weight may be given. This is to emphasise the TV minimization of non-edge region. In case of a larger difference between the neighbour and the pixel, a weaker weight may be given to better preserve the edge region of the to-be-reconstructed image. This diffusion type weighting process controls the influence of different neighbours according to the corresponding gradient. The effectiveness of the algorithms which employed this weighting process for the edge preservation is shown in a number of research studies [16] [29] [30].

However, the AwTV norm introduces another parameter ,δ, into consideration. This is added to a long list of initial parameters required for TV regularization algorithms. In the same way as other parameters, the sensitivity of this δ parameter will also be analysed in this study.

2.3. Reconstruction algorithms

In this work, the proposed algorithm, AwPCSD, as well as other 3 existing algorithms are implemented for the sensitivity analysis of parameters. The details of these algorithms are explained as follows.

ASD-POCS : Adaptive-steepest-descent projection onto convex sets

The first algorithm is the TV regularization algorithm proposed by Sidky et al [12], which minimizes TV norm of the image as expressed in equation 5:

$$x^* = argmin||x||_{TV} \tag{10}$$

with subject to the following two constraints:
(A) data fidelity constraint

$$|Ax - b| \leq \epsilon \tag{11}$$

where ϵ is an error bound that defines the amount of acceptable error between predicted and observed projection data. In real practice, it is impossible to always obtain

the reconstructed image that is perfectly consistent with the data due to several factors such as modelling errors, noise and x-ray scattering [12]. Therefore, this constraint only require that the reconstructed image yields projection data that are within a given l_2 distance ϵ of the actual projection data.

(B) non-negativity constraint

$$x \geq 0 \tag{12}$$

The second constraint requires that the voxel intensity is not less than zero.

The framework of ASD-POCS iterative algorithm has two phases for each iteration. The first phase is the implementation of simultaneous algebraic reconstruction technique (SART) [21] to enforce the data-consistency according to the two constraints in equations 11 & 12. The non-negative projection is also implemented in this stage.

The second phase is the TV optimization which is performed by adaptive steepest descent method for the TV objective function in equation 10. This is to ensure that the optimization problem have minimum TV solution. The step-size of TV minimization step is adjusted to balance data consistency constraint and TV minimization by taking into account the change from SART step and utilize that step-size in the subsequent TV optimization process.

These two steps are implemented in alternation until the stopping criterion are satisfied. More detail on the stopping criterion is discussed in the next chapter. It is crucial to find a set of parameters that balance these two steps to obtain an optimal reconstructed image. The insight study of this challenging problem is conducted in this work. In the next chapter, the role of each parameter in the reconstruction algorithms are discussed in more detail.

AwASD-POCS : Adaptive-weighted ASD-POCS

The second algorithm is called AwASD-POCS which is based on the AwTV-POCS algorithm proposed by Liu at al [16]. This algorithm is slightly modified from ASD-POCS algorithm by replacing the conventional TV norm in equation 5 by the adaptive-weighted TV norm in equation 6 to preserve the edges of the reconstructed image.

PCSD: Projection-controlled steepest descent

The third algorithm is proposed by Liu et al [19]. This algorithm adapts the two-phase strategy from ASD-POCS algorithm but the step-size of steepest descent process is adaptively adjusted according to the difference in projection domain from SART step in the current iteration. By doing so, the number of parameters to be defined for this algorithm can be reduced. The steepest-descent stage of this algorithm minimizes the conventional TV norm of the to-be-reconstructed image as expressed in equation 5.

AwPCSD : Adaptive-weighted PCSD

This is the proposed algorithm in this work. It is modified from PCSD algorithm by replacing conventional TV norm in the steepest-descent step with the adaptive-weighted TV norm in equation 6. In this way, the algorithm should preserve the edges of the to-be-reconstructed images better with less number of parameters required to implement than the ASD-POCS algorithm.

The following pseudo code summarizes the structure of four TV-based regularization algorithms used for the sensitivity analysis in this work. The code presents how all the parameters are used in which part of each algorithm. The difference between each algorithm is shown with comments on the right with the hi-lights for the proposed algorithm. Each parameter and stopping criterion are explained in more detail in the next section.

Algorithm 1 Pseudo code for four TV-based regularization algorithms

while stopping criterion not met **do**
  $x = x + \beta \cdot$ SARTupdate
  $\beta = \beta \cdot \beta_{red}$

  Update α ▷ PCSD , AwPCSD
  for ng **do**
    $x = x + \alpha \cdot$ TVupdate ▷ ASD-POCS,PCSD
    $x = x + \alpha \cdot$ AwTVupdate(δ) ▷ AwASD-POCS, AwPCSD
  end for
  Update α w.r.t. r_{max} , α_{red} , ϵ ▷ ASD-POCS,AwASD-POCS

  Check stopping criterion w.r.t. x, b, ϵ, β
end while

3. Stopping criterion and parameters for TV regularization algorithms

The most challenging problem in using TV-based algorithms is the tuning of all parameters. All 4 reconstruction algorithms implemented in the sensitivity analysis is based on two-phase strategy of ASD-POCS that alternates between data-consistency and TV minimization steps. A set of parameters is needed to adjust the contributions or balance these two operations. There is no straightforward way to determine the set of parameters for the optimal reconstruction other than trial-and-error tests. Also, when reconstructing different types of images, different parameters need to be empirically chosen [18]. This process is very time-consuming. Therefore, it is useful to examine the sensitivity that the reconstruction image has to value change on these parameters, in order to know which ones to prioritize when tuning the algorithm. Ultimately, heuristics

on how to choose this parameters are desired, to minimize or completely avoid rerunning the reconstruction with different parameters.

In this work, the sensitivity analysis of parameters is implemented by observing the impact on the reconstruction performance using simulation experiments on thorax medical phantom [20]. The values of each parameter are varied in a specified range. The results are demonstrated visually and quantitatively using two image quality metrics which will be explained in more detail in the next section.

3.1. Initial parameters for TV-based reconstruction algorithms

This section compiles explanation of parameters required to implement TV regularization algorithms. The list of parameters is based on the four algorithms implemented in this study.

- *Data-inconsistency-tolerance parameter* (ϵ)

The first one is a parameter that specifies tolerance of the to-be-reconstructed image. The value of this parameter controls an impact level of potential data inconsistency on image reconstruction. It is defined as the maximum L_2 error to accept image as valid. This parameter is used as one of the checks for the stopping criterion which are discussed in detail later on in this section.

- *TV sub-iteration number (ng)*

Next parameter is TV sub-iteration number (ng). This parameter specifies how many times the TV minimization process performs in each iteration of the algorithm.

- *TV hyperparameter* (α)

This parameter is used to convert the steepest-descent step size from a fraction of a step size to an absolute image distance on the first iteration in ASD-POCS and AwASD-POCS algorithms. This parameter is not required in PCSD and AwPCSD algorithms as these two algorithms adaptively adjust the step sizes of steepest-descent according to the difference from POCS update in the projection domain.

- *Reduction factor of TV hyperparameter* (α_{red})

Also, this parameter α_{red} is only required by ASD-POCS and AwASD-POCS algorithms. If the ratio of change in the image due to TV minimization to change in the image due to SART is greater than maximum ratio of change by TV minimization to change by SART (r_{max}) and the L_2 error of image in the current iteration is greater than ϵ,simultaneously, the gradient-descent step-size is reduced by α_{red}.

- *Relaxation parameter* (β)

This is a relaxation parameter at which the SART operator depends on. The parameter starts at 1.0 and slowly decreases to 0.0 depending on the parameter β_{red}.

• *Reduction factor of relaxation parameter (β_{red})*

This parameter is used to reduce relaxation parameter (β) in the SART step as the iteration progresses. When relaxation parameter (β) reduces to less than 0.005, the algorithm stops as it meets the stopping criterion in equation 14.

• *Maximum ratio of change by TV minimization to change by SART (r_{max})*

As mentioned in the part of parameter α_{red}, if the ratio of the change in the image due to steepest descent to the change in the image due to POCS is greater than r_{max} , the gradient-descent step-size is reduced by α_{red}.

• *Scale factor for adaptive-weighted TV norm (δ)*

This parameter is only required in adaptive-weighted algorithms i.e. AwASD-POCS and AwPCSD. It controls the strength of the diffusion in the adaptive-weighted TV norm in equation 6 during each iteration [22]. The weights in equation 6 make it possible to consider the gradient of the desired image and to take into account the changes of local voxel intensities. The adaptive-weight TV norm in equation 6 can be seen as a special case of the conventional TV norm in equation 5. When the weight is set to 1 i.e. $\delta \to \infty$, the AwTV norm is similar to the conventional TV norm.

3.2. Stopping criterion

The stopping criterion play an important role in the reconstruction algorithms as they specify at which point the algorithms should be stopped. Generally speaking, the algorithms are stopped either when the difference of image between current and previous iterations is not noticeable or the image is accepted to be an optimal one. The stopping criterion utilized in the reconstruction algorithms in this paper comprise of 3 checks.

Firstly, we consider the case where reconstructed image is accepted to be an optimal solution. When implementing the algorithm, the currently estimated image is checked to see if it obeys the constraints of equations 11 and 12. Also, the TV and data-constraints gradients vectors are checked if they are back-to-back by observing the cosine of angle between them. Theoretically, the estimated image is optimal when these two vectors point exactly in opposite directions. The reader is referred to read more detailed explanation of the neccessary conditions for a given image to be the optimal one in [12].

Therefore, the first check of the stopping criterion for all four reconstruction algorithms in this work is when the currently estimated image satisfies the following conditions:

$$c < -0.99 \quad \& \quad dd \leq \epsilon \tag{13}$$

where c is the cosine of the angle between the TV and data-constraint gradients, dd is the L_2 error between the measured projections and the projections computed from the estimated image in the current iteration , ϵ is the data-inconsistency-tolerance parameter.

In an ideal scenario, the value of c should be -1 as the vectors of TV and data-constraint gradients must be completely opposite to each other. Practically, this value is difficult to reach as it requires a large number of iterations [12]. Thus, this value is set to -0.99. The algorithm is stopped when the currently estimated image satisfies these two conditions in equation 13 simultaneously.

Secondly, the iteration is ceased when the relaxation parameter (β) of the current iteration meets the following condition

$$\beta < 0.005 \tag{14}$$

The relaxation parameter reduces every iteration by a factor of specified β_{red}. When value of β falls below 0.005, no further difference is noticeable between the reconstructed images of the current and next iterations. Hence, the algorithm is forced to stop.

Last check of the stopping criterion is when the maximum number of iteration specified by user is reached. As the number of iterations is a constant and cannot be updated adaptively, the algorithm may be stopped either before or after the optimal solution is obtained.

When the algorithm meets any of these three stopping criterion checks, the current iteration is ceased and the currently estimated image is accepted to be a final reconstructed image.

4. Results

In this section, two objectives of the proposed work are analysed. Firstly, the sensitivity analysis is conducted for a set of parameters required for TV minimization-based reconstruction algorithms. The aim is to examine the sensitivity that the reconstructed image has to value change on the parameters, in order to know which ones to prioritize when tuning the algorithm. Ultimately, heuristics on how to choose the parameters are desired, to minimize or completely avoid rerunning the reconstruction with different parameters.

Secondly, the proposed algorithm , AwPCSD, is evaluated in comparison to 3 existing algorithms : ASD-POCS, AwASD-POCS and PCSD on X-ray CT reconstruction. All the algorithms are implemented based on the algorithms available in Tomographic Iterative GPU-based Reconstruction (TIGRE) toolbox [23] proposed by Biguri et al. The ASD-POCS algorithm used in this study is utilized from the TIGRE toolbox while the other three algorithms are modified and implemented based on the algorithms available in this toolbox. Also, we are looking to investigate how the adaptive-weighted function help to improve the result by comparing between two pairs of adaptive-weighted and non-adaptive-weighted algorithms.

The data set used to evaluate the performance of reconstruction algorithms and parameters analysis is a digital XCAT phantom which contains thorax anatomy structures [20]. The Poisson and Gaussian noise [24], [25] has been added to the input

projection data for a simulation of realistic noise. Figures [1a] and [1b] show one cross-sectional slice of exact thorax phantom and the region of interest used to compute the evaluation metrics, respectively.

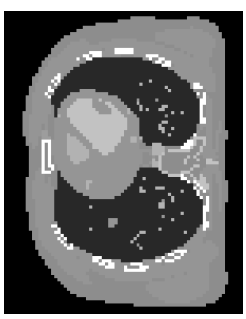

(a) Exact phantom

(b) Region of interest

Figure 1: One cross-sectional slice of thorax phantom data set

Number of projection views used to reconstruct an image in this study is 20 views which are equally sampled from 360 degrees angle. For these few numbers of projections, reconstruction using standard FDK algorithm can give an extremely poor quality reconstructed image with streak artifacts as shown in the figure 2.

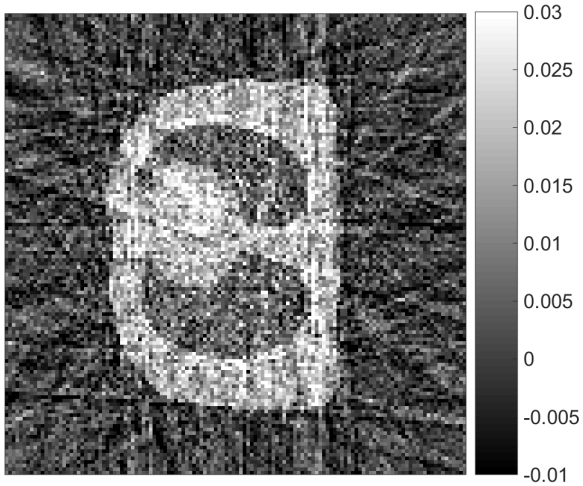

Figure 2: Reconstructed images from 20 projection views using FDK method

With this limited data scenario, the performance of the purposed AwPCSD algorithm as well as other three existing TV-based reconstruction algorithms can be intensively evaluated and compared. The following two metrics were used as a quantitative measure of reconstruction quality in this study.

4.1. Image Quality Metrics

• Root mean squared error (RMSE)

The first metric is root mean squared error (RMSE) which calculates the similarity between the resulting image and the reference image. The RMSE is defined as follows [26]:

$$RMSE = \sqrt{\frac{1}{N}\sum_{i=1}^{N}(\hat{f}(x_i) - f(x_i))^2} \tag{15}$$

where $\hat{f}(x_i)$ represents the reference attenuation coefficient at voxel i , $f(x_i)$ represents the reconstructed attenuation coefficients at voxel i, N is total number of voxels of the image. A small value of RMSE indicates small difference between the two images and vice versa.

• Correlation coefficient (CC)

The second metric is correlation coefficient (CC) which measures the degree to which the two images are associated. The CC metric is defined as follows

$$CC = \frac{Cov(\hat{f}(x), f(x))}{\sigma_{\hat{f}(x)}\sigma_{f(x)}} \tag{16}$$

where $Cov(\hat{f}(x), f(x))$ is the covariance of the reference and reconstructed images, $\sigma_{\hat{f}(x)}$ is the standard deviation of the reference image, $\sigma_{f(x)}$ is the standard deviation of the reconstructed image. The value of CC is between -1 and 1 where 1 is the total positive linear correlation, 0 is no linear correlation and -1 is total negative linear correlation.

4.2. Sensitivity analysis of parameters

This section analyses a sensitivity of all the parameters required for 4 reconstruction algorithms: ASD-POCS, AwASD-POCS, PCSD and AwPCSD. Each parameter is analysed separately across all the algorithms. The RMSE and CC values calculated from final estimated images from each value of parameter are plotted to see the performance of 4 algorithms in respond to changing of parameters' values.

The total number of parameters is different among the 4 algorithms in this study. The table 1 shows the set of initial parameters for each algorithm that is used as a starting point to analyse the sensitivity of the first parameter, ϵ.

Table 1: A set of initial parameters for the sensitivity analysis

Algorithms	ng	α	α_{red}	β	β_{red}	r_{max}	δ
ASD-POCS	25	0.002	0.95	1	0.98	0.94	N/A
AwASD-POCS	25	0.002	0.95	1	0.98	0.94	0.001
PCSD	10	N/A	N/A	1	0.98	N/A	N/A
AwPCSD	10	N/A	N/A	1	0.98	N/A	0.001

According to the above table, the ASD-POCS algorithm which is used as a reference algorithm requires 7 parameters including ϵ. The AwASD-POCS requires one more parameter from ASD-POCS which is δ as it implements the adaptive-weighted TV norm, making AwASD-POCS the algorithm that requires highest number of parameter among the 4 algorithms. The PCSD and AwPCSD algorithms require three less parameters than ASD-POCS and AwASD-POCS algorithms including α, α_{red} and r_{max}, making PCSD the algorithm that requires the least number of parameters among all 4 algorithms.

Data-inconsistency-tolerance parameter (ϵ) The first parameter to be analysed is ϵ. This parameter is required by all 4 algorithms and significant to the final reconstructed image as it involves in stopping criterion of equation 13.

To begin the sensitivity analysis, the other parameters are set to their initial settings while ϵ values are varied from 0 to 10^5. The RMSE and CC values are calculated using the reconstructed image obtained from each ϵ value and plotted as shown in figure 3.

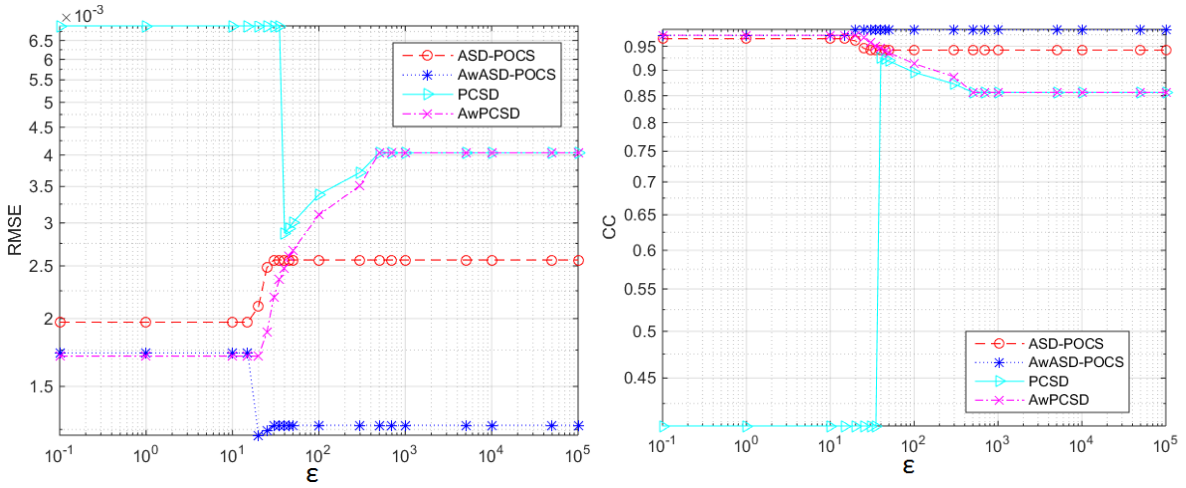

(a) RMSE plots from varying ϵ

(b) CC plots from varying ϵ

Figure 3: RMSE and CC plots across different ϵ values

Considering the pair of PCSD and AwPCSD algorithms in figure 3a, the RMSE values of reconstructed images from PCSD are very high when ϵ are in the low values

range below 40 which result in a poor quality image as shown in the second row of figure 4 when $\epsilon = 0$. This is because the auto-selecting of steepest-descent step-size of PCSD leads to sometimes wrong values and unpredictable stopping. However, when looking at the same range of ϵ for AwPCSD, it performs significantly better than PCSD with only the adaptive-weighted function added on to PCSD algorithm.

Now turning to the pair of ASD-POCS and AwASD-POCS algorithms. At the low range of ϵ values, both algorithms perform relatively well with slightly lower RMSE values for AwASD-POCS. This can be seen in the figure 4 for $\epsilon = 0$ and 40 that the adaptive-weighted function of AwASD-POCS can recover small details of the object better than ASD-POCS algorithm. When the ϵ is larger, the RMSE of ASD-POCS become larger and the quality of image deteriorates. In case of AwASD-POCS, the algorithm behaves differently. The RMSEs of reconstructed images from large ϵ are lower than those of the small ϵ. This is analysed further and found that all the iterations from AwASD-POCS in this particular study are ceased solely because the β stopping criteria is met, following equation 14. It means that the behaviour being observed here for AwASD-POCS is not thoroughly the effect of varying just the values of ϵ, as the stopping criteria for the L_2 norm error in equation 13 is not met. However, the study of correlation between a group of parameters would be complicated and is beyond the scope of this work.

Comparing between the two pairs of adaptive-weighted and non-adaptive-weighted algorithms, we can see that the adaptive-weighted function makes the algorithms more robust and more stable to the parameter changes. This can be seen from the RMSE values of the AwASD-POCS and AwPCSD algorithms which are lower than those of ASD-POCS and PCSD algorithms over the same range of ϵ.

The visual inspection also follows this conclusion as can be seen from figure 4. The AwPCSD and AwASD-POCS outperformed the other 2 algorithms in all cases especially when the ϵ is in the low range i.e. when $\epsilon = 0$ and 40. As the ϵ increases, the performance of AwASD-POCS becomes more stable than AwPCSD and remains robust over the entire range of ϵ values under study.

It is very difficult to identify any specific value as the most appropriate ϵ for one particular data set as the ϵ is data-specific. However, from the trials and errors, we can suggest that using the L_2 norm of the reconstructed image obtained from Ordered-subset simultaneous algebraic reconstruction techniques (OS-SART) algorithm [27] as ϵ gives an acceptable result. However, one has to bear in mind that specifying the ϵ is a matter of image quality versus computational time. Choosing too small ϵ might take longer computational time to achieve the desired value and also does not guarantee the best image for some of the algorithms. This can be seen from figure 3a that stopping criterion of reconstructed images with ϵ lower than 20 is from reaching the maximum number of iterations which takes long computational time. Moreover, in case of PCSD and AwASD-POCS algorithms, the reconstructed images from larger ϵ even have better quality with smaller RMSE values.

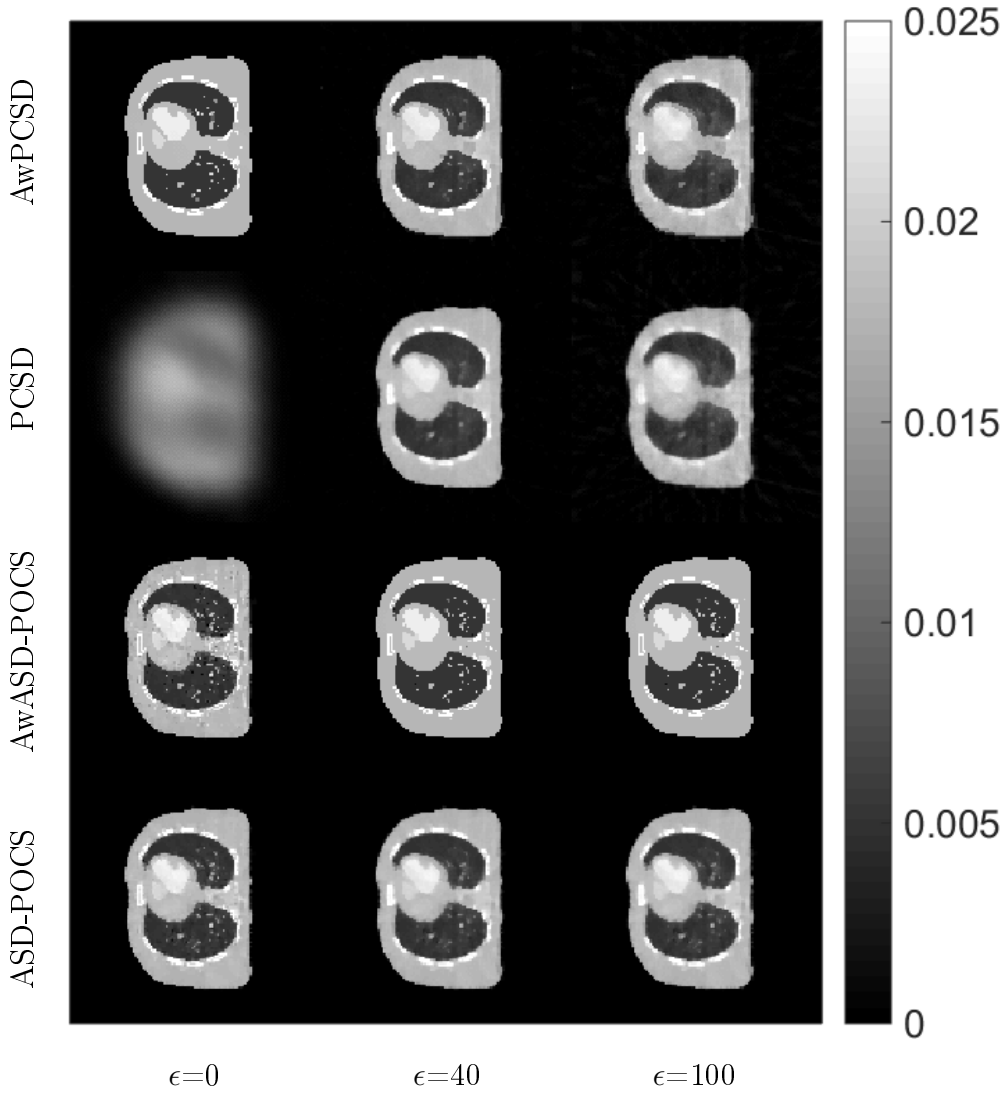

Figure 4: Reconstructed images from 4 algorithms using different ϵ values

TV sub-iteration number *(ng)* The second parameter is TV sub-iteration number. This parameter is varied from 1 to 200. Other parameters are still the same as initial settings apart from ϵ which are chosen to be the optimal values for each algorithm obtained from the previous section.

According to the RMSE plot in figure 5a, two algorithms which achieve the lowest RMSE values are AwASD-POCS and AwPCSD.

Firstly, we consider the pair of PCSD and AwPCSD algorithms. For PCSD algorithm , the reconstructed images from low number of TV sub-iteration are still acceptable even though the images are not very clear as seen from the second row of figure 6. When the TV sub-iteration number increases, the RMSE values suddenly go up with relatively bad reconstructed images when $ng > 10$. This is to show that the strange performance of PCSD algorithm arises very easily, following on from sensitivity of ϵ to TV sub-iteration number in this case. However, with the adaptive-weighted function

added on to PCSD algorithm, the AwPCSD algorithm can significantly improve the quality of reconstructed images as the TV sub-iteration number increases. The lowest RMSE value of the reconstructed images from AwPCSD is when $ng = 6$. After that, the reconstructed images get more blurred with the increasing TV sub-iteration number as seen in the first row of figure 6.

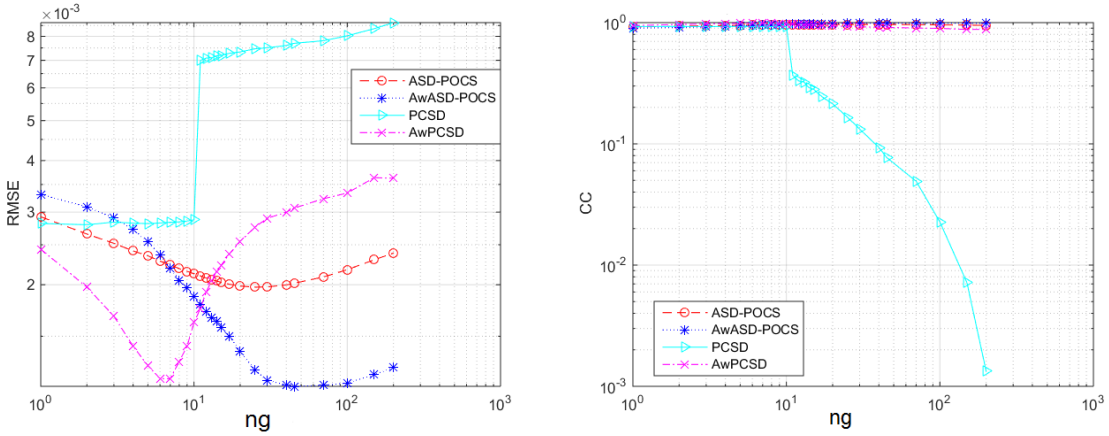

(a) RMSE plots from varying ng (b) CC plots from varying ng

Figure 5: RMSE and CC plots across different ng values

Analysing the pair of ASD-POCS and AwASD-POCS algorithms, both algorithms improve the quality of reconstructed images as the TV sub-iteration number increases until they reach their lowest RMSE points which differ in both algorithms. For the ASD-POCS, the algorithm hits the lowest RMSE point when ng is approximately between 20 to 50. The AwASD-POCS algorithm is still able to bring down the RMSE further from the point of ng approximately equals to 6 until it reaches the lowest point when ng is between 30 to 100.

The two adaptive-weighted algorithms, AwASD-POCS and AwPCSD, can bring down the RMSE of the final reconstructed images to approximately the same level. According to figure 5a, the AwPCSD requires less TV sub-iteration number than AwASD-POCS to reach the optimal reconstructed image which can save significant amount of computational time. This is because the AwPCSD algorithm takes into account the current image error when choosing the TV steepest descent step-size for the next iteration. However, the AwPCSD is more sensitive to the changing values TV sub-iteration number as the quality of final reconstructed images deteriorate quickly with the increasing ng as shown in the figure 6.

To sum up, the adaptive-weighted algorithms outperformed the non-adaptive-weighted algorithms over the range of TV sub-iteration numbers under study. Comparing between AwPCSD and AwASD-POCS, although the best reconstructed images from these 2 algorithms achieve the same level of RMSE, AwPCSD algorithm requires less number of ng which save computational time. However, it is important to

specify a proper TV sub-iteration number when implementing AwPCSD algorithm as this algorithm is very sensitive to values change.

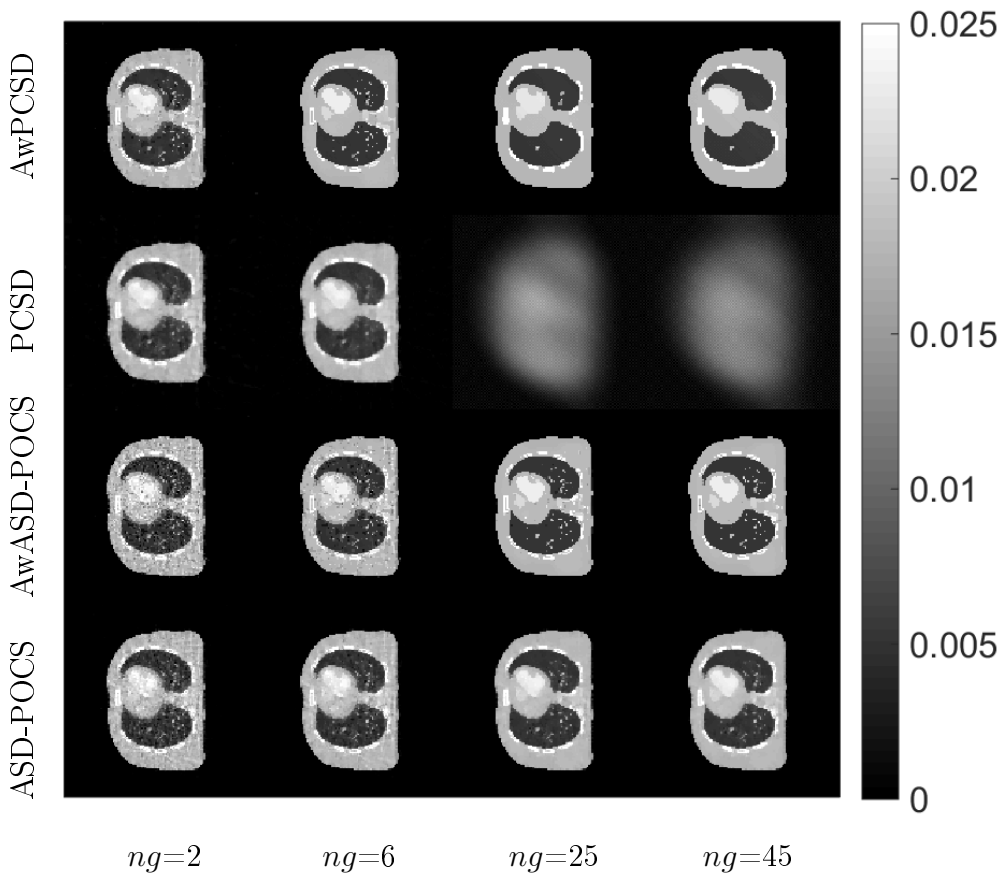

Figure 6: Reconstructed images from 4 algorithms with different ng values

TV hyperparameter ***(α)*** The next parameter to be studied is α. This parameter is only required by ASD-POCS and AwASD-POCS algorithms. In these 2 algorithms, the α is used to specify the steepest-descent step-size in the first iteration. As the iteration goes on, the TV step-size will be reduced by the amount of α_{red} if the condition which we briefly discussed in the part of data-inconsistency-tolerance ϵ parameter section is met.

The α parameter is varied from $0, 2 \times 10^{-8}, 2 \times 10^{-5}, 2 \times 10^{-4}, 2 \times 10^{-3}, 0.1, 1, 5, 10$ to 20. Other parameters are still the same as initial settings apart from ϵ and ng which are set as found in the previous sections. The RMSE and CC plots of final reconstructed images using different α values over the range of study are shown in figure 7.

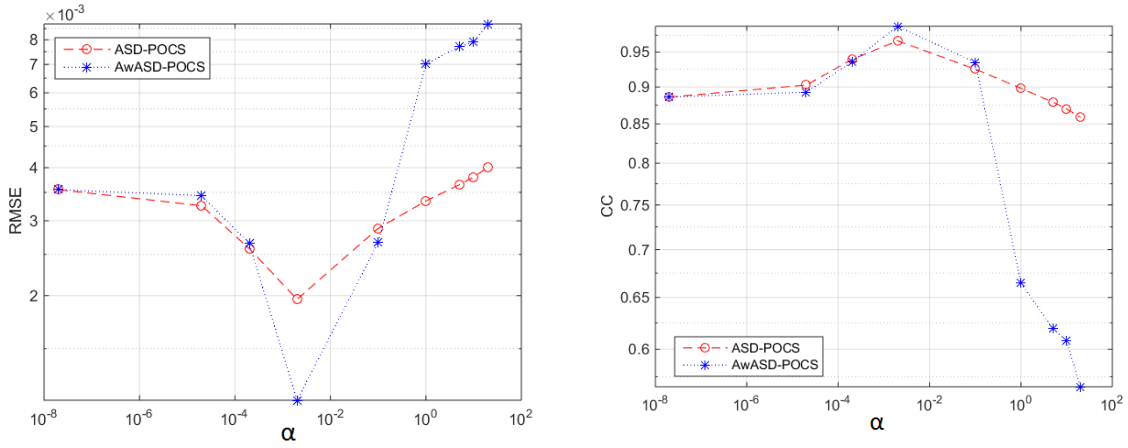

(a) RMSE plots from varying α

(b) CC plots from varying α

Figure 7: RMSE and CC plots across different α values

From the RMSE plots, both algorithms have a minima in a very specific value of α i.e. when $\alpha = 0.002$. The reconstructed images get increasingly deteriorated the further away the α is from that value. This can be seen from the reconstructed images in figure 8. Again, the AwASD-POCS algorithm has better performance than ASD-POCS algorithm with the clearer reconstructed image in the same value of α.

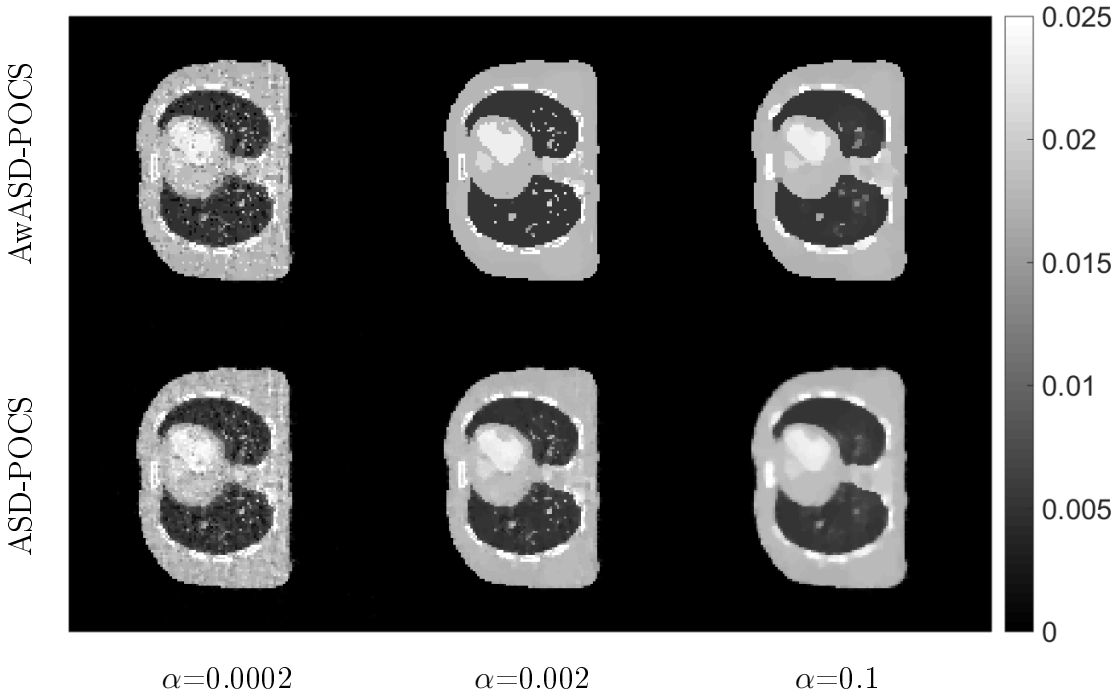

Figure 8: Reconstructed images from ASD-POCS and AwASD-POCS with different α values

Therefore, it is of the utmost importance to specify a proper value of α for the

ASD-POCS and AwASD-POCS algorithms to work properly. With this knowledge, we can say that this is a great advantage of PCSD and AwPCSD algorithms that do not require this α parameter

Reduction factor of TV hyperparameter (α_{red}) In the same way as α, the α_{red} parameter is only required by two algorithms, ASD-POCS and AwASD-POCS. This parameter is involved in the condition which has been discussed briefly earlier. For the next iteration, the gradient-descent step-size is reduced by α_{red} only when the ratio of change due to TV minimization to change due to SART is greater than r_{max} and the L_2 error of image in the current iteration is greater than ϵ simultaneously.

The range of α_{red} being studied here is varied from 0.1 to 1. The RMSE and CC plots of final reconstructed images using different α_{red} values over this range are shown in figure 9.

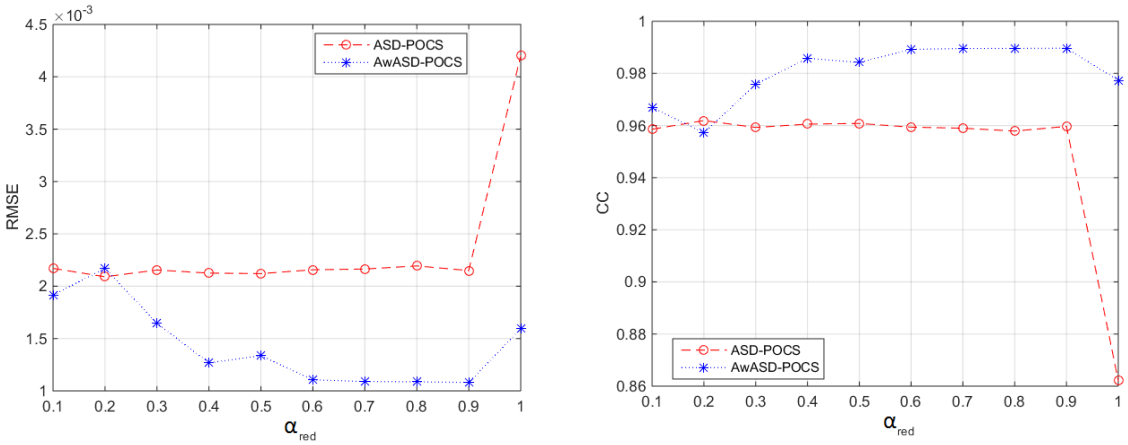

(a) RMSE plots from varying α_{red}

(b) CC plots from varying α_{red}

Figure 9: RMSE and CC plots across different α_{red} values

Considering RMSE and CC plots, the reconstructed images obtained from AwASD-POCS with different α_{red} achieve lower RMSE values and higher CC values than that of the ASD-POCS in almost all cases. Again, this is also showing that the adaptive-weighted function can significantly improve the quality of the reconstructed images.

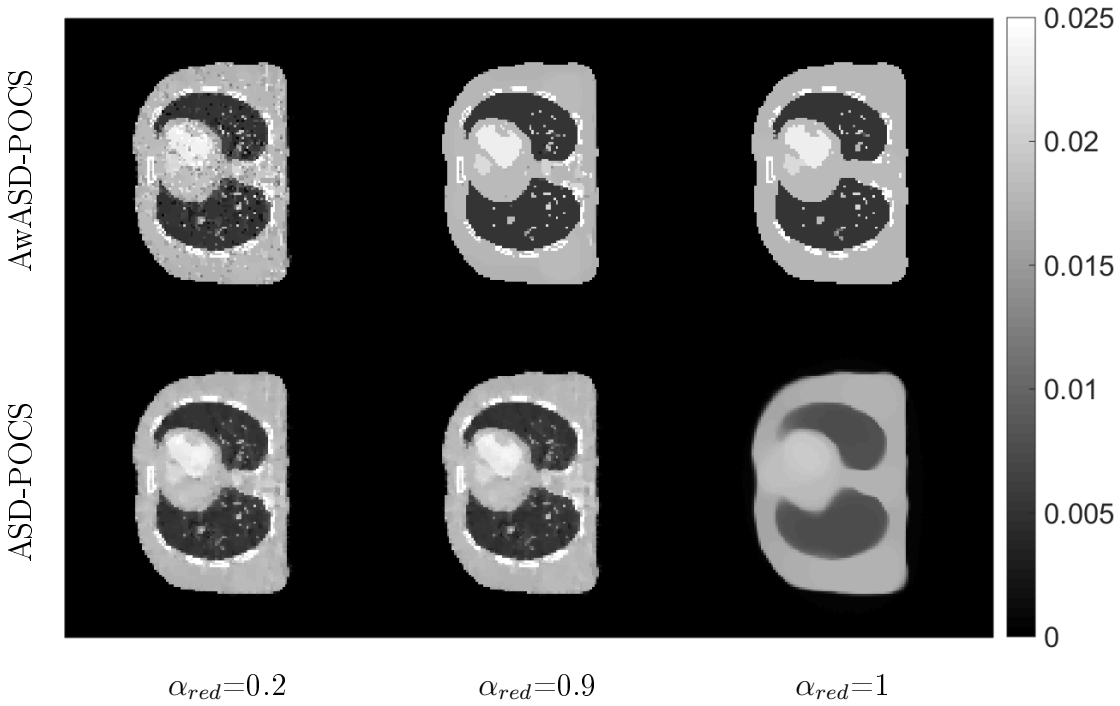

Figure 10: Reconstructed images from ASD-POCS and AwASD-POCS with different α_{red} values

From this study, we can see that the α_{red} parameter is a sensitive parameter especially when increasing from 0.9 to 1. It is a crucial parameter to set to a proper value. For both algorithms, reduction of α is crucial. Therefore, the α_{red} should not be set to 1 as the quality of image is deteriorated hugely. The suggested value of α_{red} for the implementation of ASD-POCS and AwASD-POCS is any value close to 1 for the best results.

As this α_{red} parameter is sensitive to value change and requires a proper setting, it is another advantage of PCSD and AwPCSD algorithms that these 2 algorithms do not require this parameter for their implementations.

Relaxation parameter (β) This is the parameter that defines how strong the effect of SART function have to the current iteration of the reconstruction. Many existing works have studied and suggested several ways to choose the optimal value for relaxation parameter [28].

In this study, the relaxation parameter is varied from 0 to 1. According to the RMSE plot in figure 11a, when $\beta = 0$, all 4 algorithms have high level of RMSE which is expected as SART operation is suppressed. As β increases to 1, the quality of reconstructed images is gradually improved with lower RMSE for all algorithms apart from PCSD where the RMSE values increase in the middle part of the range. Although the RMSE of reconstructed images with β closer to 1 are slightly different, the quality of images is not that significantly improved. Thus, the recommended setting for β

parameter is 1.

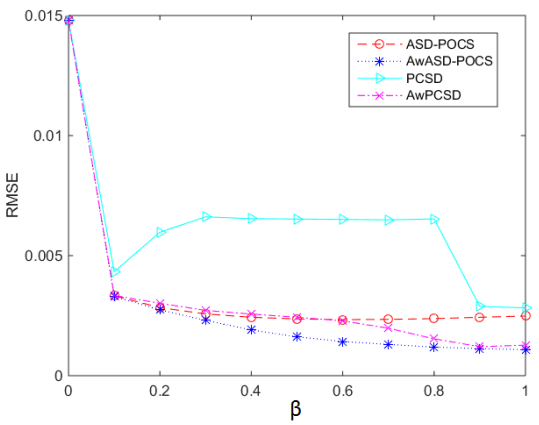

(a) RMSE plots from different β

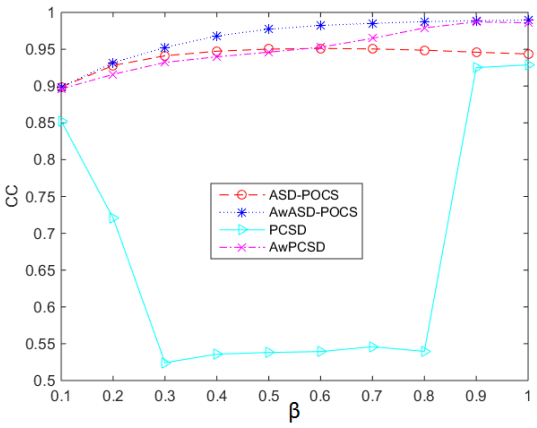

(b) CC plots from different β

Figure 11: RMSE and CC plots across different β values

Reduction factor of relaxation parameter (β_{red}) This parameter is varied from 0.1, 0.2, 0.3, 0.4, 0.5, 0.6, 0.7, 0.8, 0.9, 0.98, 0.99 to 1. The value of $\beta_{red} = 1$ means that the same amount of effect from SART operation is kept constant as the iteration goes on. Decreasing β_{red} from 1 to 0.1 reflects in less and less amount of relaxation parameter β for the next iteration.

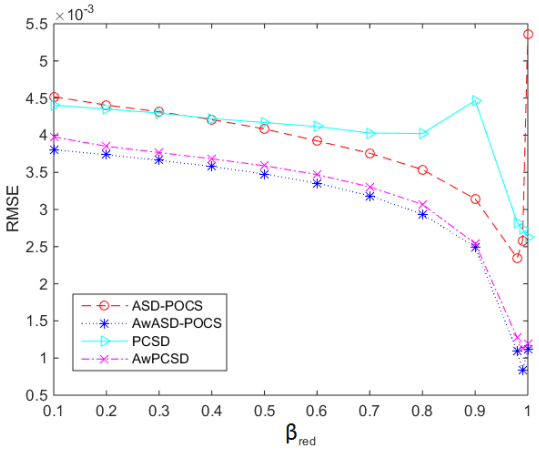

(a) RMSE plots from different β_{red}

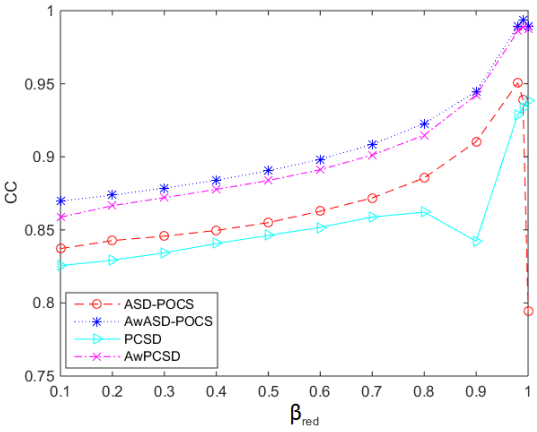

(b) CC plots from different β_{red}

Figure 12: RMSE and CC plots across different β_{red} values

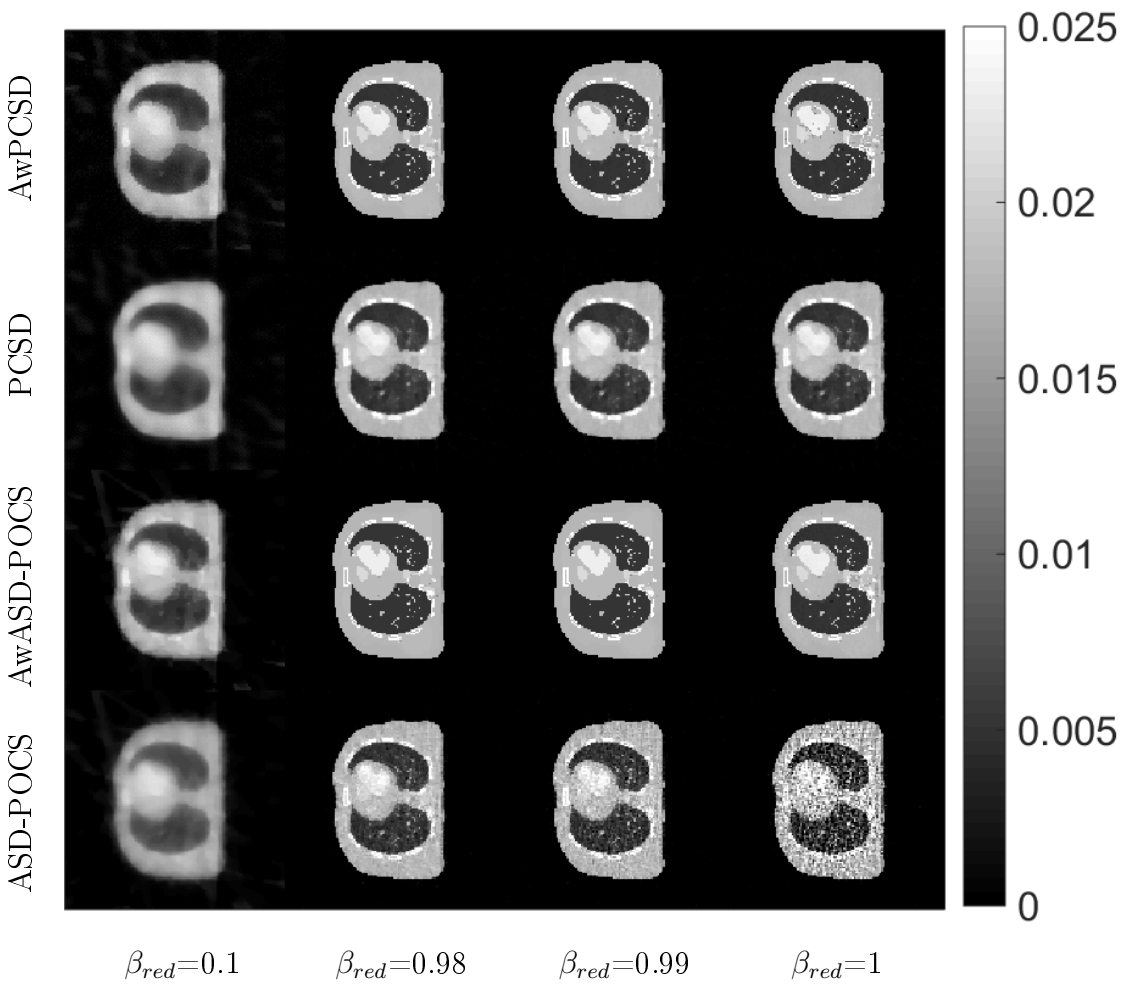

Figure 13: Reconstructed images with different β_{red} values

From the RMSE and CC plots in figure 12, we can see that values of RMSE are the lowest when β_{red} are close to 1. The quality of reconstructed images quickly deteriorate as the β_{red} get smaller upto 0.1 as can be seen from the cross-sectional slices of the reconstructed images in figure 13.

From this study, the suggested range of β_{red} is value larger than 0.98 but smaller than 1 to ensure the effect of SART operation is reduced for the next iteration but not excessive.

Maximum ratio of change by TV minimization to change by SART (r_{max})
The r_{max} parameter is required by two algorithms: ASD-POCS and AwASD-POCS. This parameter is also involved in the condition for TV steepest-descent step-size adaptation for next iteration. If the ratio of the change in the image due to steepest descent to the change in the image due to POCS is greater than r_{max} , the gradient-descent step-size is reduced by α_{red}. In case that the current image satisfies the data-inconsistency-tolerance condition, the gradient-descent step-size is then no longer reduced.

From this condition, we can see that the reconstructed images obtained from varying

r_{max} also depends on the values of ϵ and α_{red}. However, the study of combination of parameter would be too complex to evaluate.

The r_{max} in this study is varied from 0, 0.1, 0.2, 0.3, 0.4, 0.5, 0.6, 0.7, 0.8, 0.9, 0.94, 1, 2, 3, 4 to 5. The RMSE and CC plots of the reconstructed images obtained from varying r_{max} in this range is shown in figure 14.

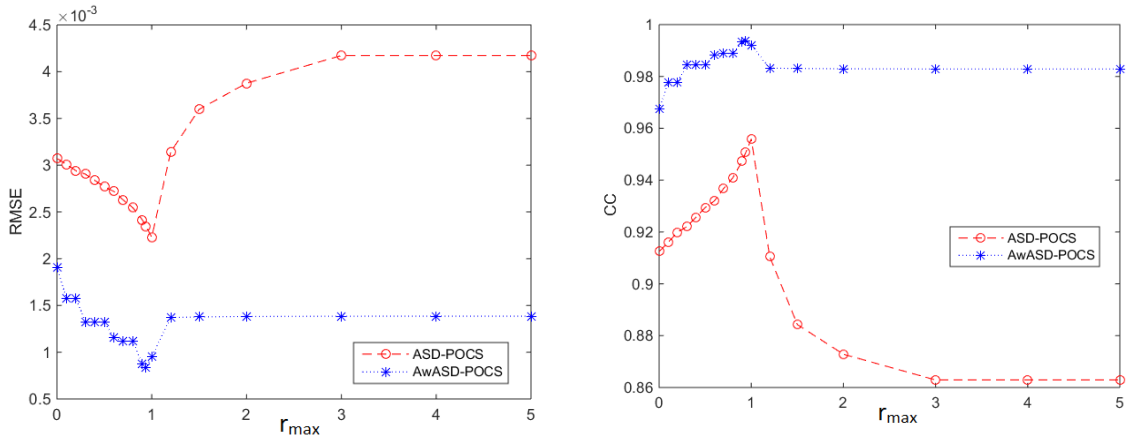

(a) RMSE plots from different r_{max}

(b) CC plots from different r_{max}

Figure 14: RMSE and CC plots across different r_{max} values

According to figure 14, the best results for both algorithms are from $r_{max} = 1$ which means that the algorithms best perform when the change in the image is balanced between the two operations. In other words, the ratio of the change in the image due to steepest descent should be equal to the change in the image due to SART

As in the previous sections, the introduction of the adaptive-weighted TV norm results in overall a better image.

Scale factor for adaptive-weight TV norm (δ) This parameter is only required by AwASD-POCS and AwPCSD algorithms that implement adaptive-weighted TV norm as expressed in equation 6. The δ parameter is a scale factor controlling the amount of smoothing being applied to the image voxel at edges relative to non-edge region during each iteration.

Figure 15 shows the weight function plot from the weight equations 7-9. The range of image gradient in X axis is specified from 0 to 0.01 with six values of δ : $0.0005, 0.001, 0.003, 0.005, 0.01, 0.1$. The RMSE and CC values obtained from the reconstructed images of different values of δ are plotted in figure 16.

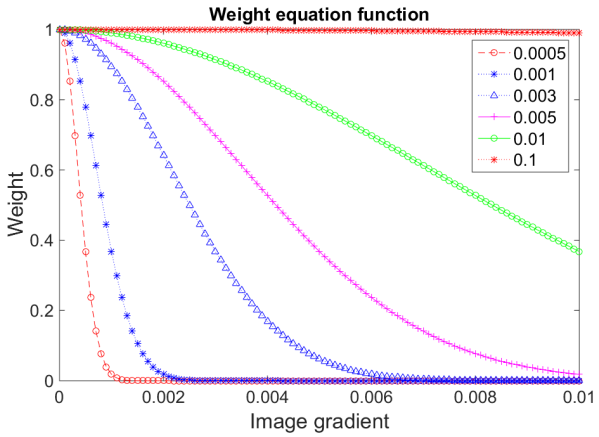

Figure 15: Weight equation function

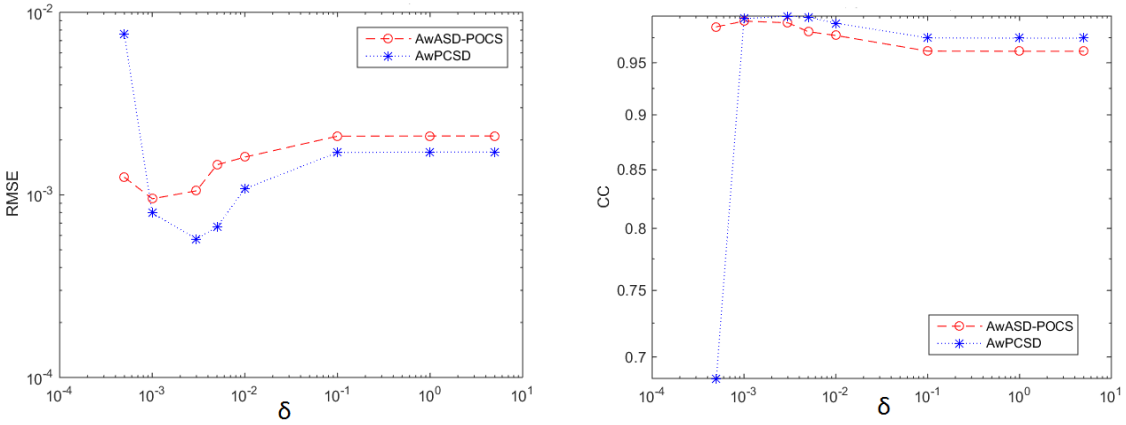

(a) RMSE plots from different δ

(b) CC plots from different δ

Figure 16: RMSE and CC plots across different δ values

According to figure 15, the weight equation with a small value of δ specifies low weights to almost every pixels. This means that the algorithm preserves most of the gradient by letting TV minimization have less influence to its implementation . Hence, the reconstructed images will be on the noisy side as can be seen from the figure 17 especially the case of AwPCSD with $\delta = 0.0005$.

On the other hand, when δ is large, the function specifies high weights to almost every gradient size of image. This allows TV minimization to have more influence during the implementation of the algorithm results in the blurred side of the image.

Setting values of δ to these 2 extreme cases makes the algorithm unable to differentiate between the noise which normally have small gradient and the edges which have larger gradient. The appropriate setting of δ is significant to the adaptive-weighted algorithms as it will allow TV minimization to have more influence to remove noise and less influence to preserve edges.

A proper choice of δ is specific to each data set. The suggested way to choose δ is by setting it to approximately 90th percentile of histogram of the reconstructed image from

OS-SART algorithm. The weight equation function can be plotted using this value of δ to see how much influence of TV minimization is preferred for different level of image gradient.Minor alternation might be needed around this value to ensure that the weight equation can preserve the gradient of the edges while removing the potential noise of the image.

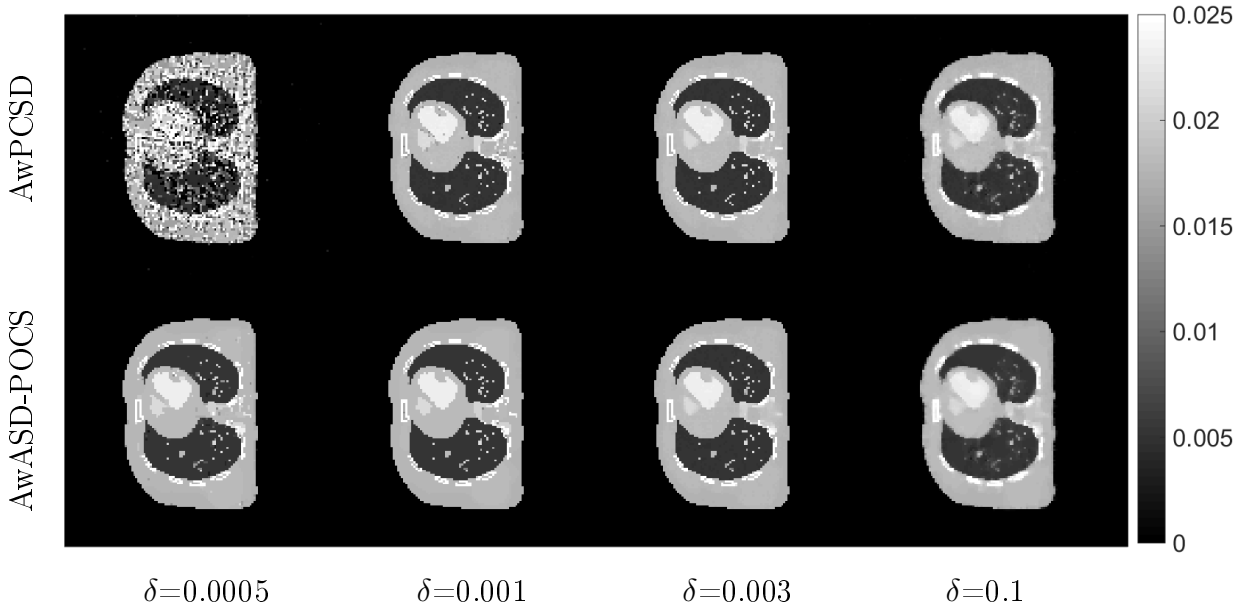

Figure 17: Reconstructed images from different δ values

After the sensitivity analysis of all the parameters has been implemented, figure 18 shows the cross-sectional slices of reconstructed images from the best possible setting of parameters obtained from the analysis. It is clearly seen that the AwPCSD algorithm can preserve the edges of reconstructed image better than other 3 algorithms.

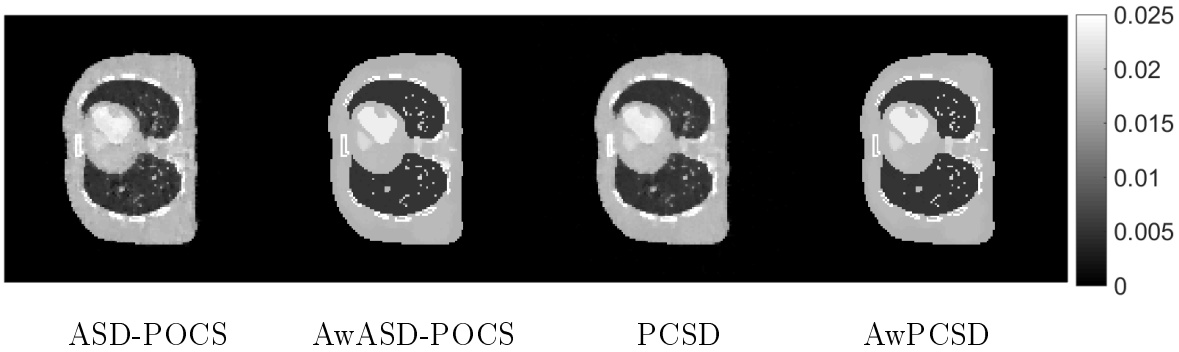

Figure 18: The cross-sectional slices of reconstructed images of 4 algorithms from the best set of parameters.

4.3. Further analysis of the reconstructed images

In order to analyse the edge preserving property of the experimental results, the image profiles along the horizontal and vertical lines as shown in the figure 19 are plotted.

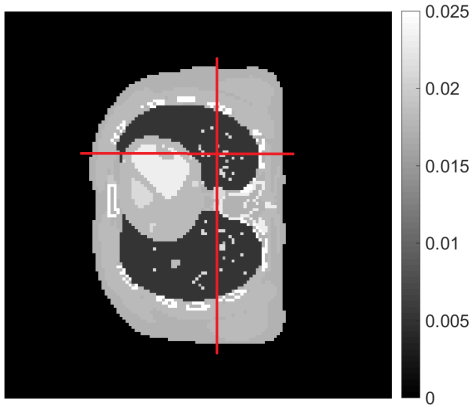

Figure 19: The image profiles are plotted along the horizontal and vertical lines.

The profiles of reconstructed images from the 4 algorithms are plotted in figure 20 with reference to the Thorax phantom. This is to compare the ability of the reconstruction algorithms to reconstruct the small features as well as preserving the edges of the phantom.

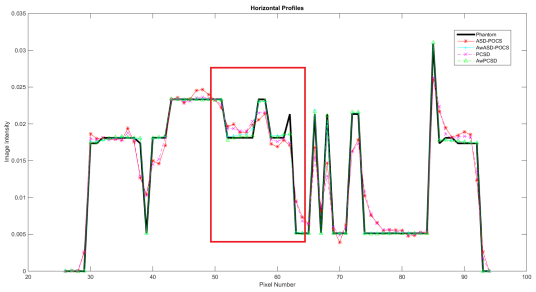

(a) The image profiles along the horizontal line.

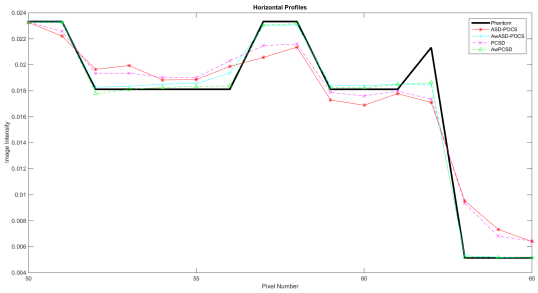

(b) Partial profiles of the selected ROI.

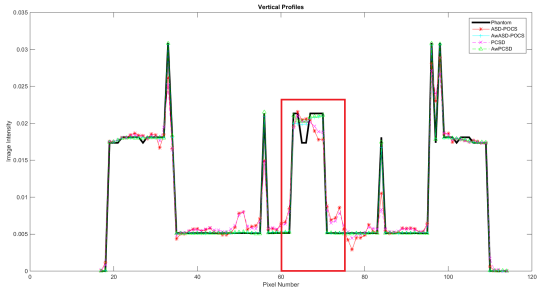

(c) The image profiles along the vertical line.

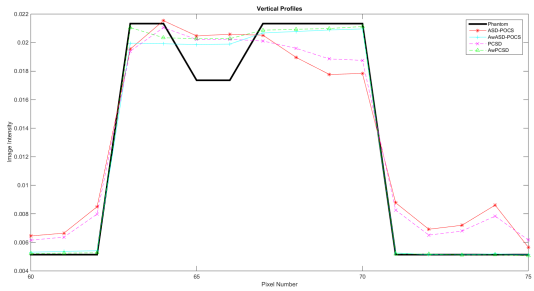

(d) Partial profiles of the selected ROI.

Figure 20: 1D profiles along the horizontal line (81st row of the reconstructed images) and the vertical line (71st column of the reconstructed images.)

The 1D profiles of the true phantom are plotted in solid black line for reference.

Region of interest (ROI) is selected from 1D profiles and marked by the red rectangles in the left column of the figure 20. The profiles of these selected pixels are plotted in the right column to observe the differences clearer. It can be obviously seen that the profiles of the adaptive-weighted algorithms i.e. AwASD-POCS and AwPCSD show better alignment with the true phantom than those of the ASD-POCS and PCSD algorithms.

Comparing between the two adaptive-weighted algorithms: AwASD-POCS and AwPCSD, although the differences between these two methods are not clearly visible,the reconstructed image from AwPCSD shows a slightly better alignment with the true phantom than that of the AwASD-POCS algorithm.

5. Experimental evaluation

SophiaBeads dataset

Apart from the simulated data set, the proposed algorithm is also tested with the real microCT datasets, The SophiaBeads Datasets [31]. The sample is a plastic tube with a diameter of 25 mm, filled with uniform Soda-Lime Glass (SiO_2-Na_2O) beads of diameters 2.5 mm (with standard deviation 0.1 mm). The dataset is loaded using the scripts in the project [32]. The source-to-detector distance is 1.007×10^3 mm and the source-to-object distance is 80.6392 mm. The detector size is 1564 x 1564 pixels and the image size is 1564 x 1564 x 200 voxels. The number of projections used to reconstruct the image in this experiment is 64 projections.

The gold standard image used as a reference in this study is reconstructed by FDK algorithm with 2048 projections. The proposed algorithm, AwPCSD, is tested with this dataset as well as other 3 TV-based regularization algorithms and FDK for a comparison. The set of parameters used for each TV-based algorithm is derived as suggested in the results section. The detail of each parameter is explained in table 2

Table 2: The optimum set of parameters used for SophiaBeads dataset

Algorithms	ϵ	ng	α	α_{red}	β	β_{red}	r_{max}	δ
ASD-POCS	1.5e+04	25	0.002	0.9	1	0.99	1	N/A
AwASD-POCS	1.5e+04	45	0.002	0.9	1	0.99	1	0.1129
PCSD	1.5e+04	6	N/A	N/A	1	0.99	N/A	N/A
AwPCSD	1.5e+04	6	N/A	N/A	1	0.99	N/A	0.0922

The optimum set of parameters used in this SophiaBeads dataset have some similarities and differences compared to the one used for Thorax phantom dataset.

The parameters such as TV sub-iteration (ng), TV hyperparameter (α), Reduction factor of TV hyperparameter (α_{red}) , Relaxation parameter (β), Reduction factor of relaxation parameter (β_{red}) and Maximum ratio of change by TV minimization to change by SART (r_{max}) are similar, whereas data-inconsistency-tolerance (ϵ) and Scale factor for adaptive-weight TV norm (δ) are different. The latter two parameters are defined specifically for each dataset based on the method suggested in the paper with some small modification.A cross-sectional slice of the reconstructed images from each algorithm is shown in figure 21.

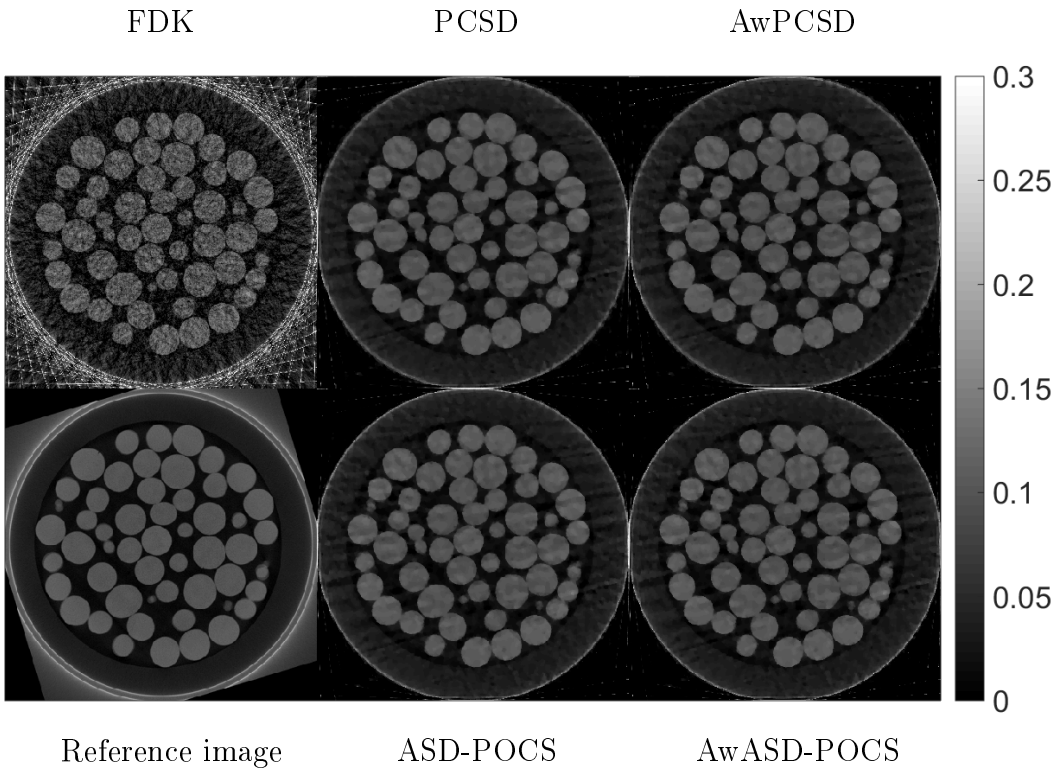

Figure 21: The cross-sectional slices of reconstructed images from SophiaBeads datasets.

The FDK algorithm performs rather badly in this limited data scenario. The reconstructed images from TV-based reconstruction algorithms have less artefacts, but look very similar from one algorithm to another. To observe the difference of each algorithm better, the image profiles along the horizontal line as shown in figure 22a are plotted to compare the edge preserving property. The horizontal image profile along the 146th row is plotted in figure 22b with the ROI between 305th to 325th column as shown in figure 22c.

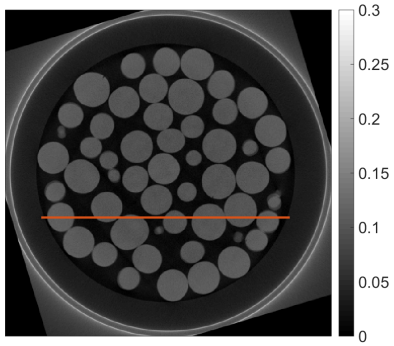

(a) Horizontal line through the 146th row of the image

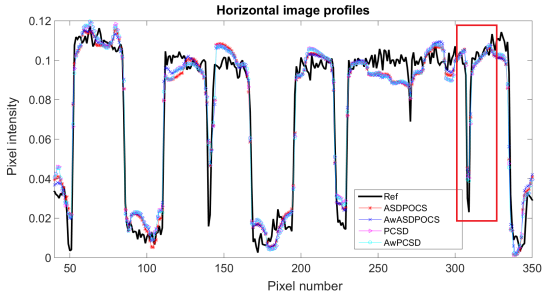

(b) The image profiles along the horizontal line

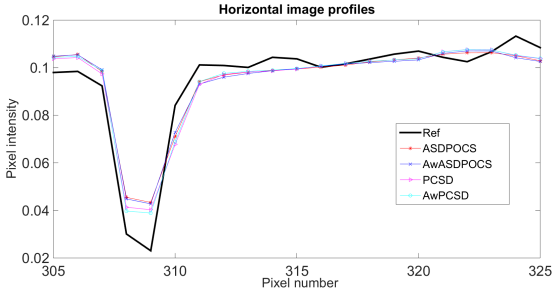

(c) Partial profiles of the selected ROI

Figure 22: The reconstructed images profiles

Considering the 1D profile plot of the ROI in figure 22c, the reconstructed images from 4 algorithms have very similar image profiles. However, the result from the proposed AwPCSD algorithm is closer to the reference image in some parts, especially when the pixel intensity is lowering down approximately near the pixel number 308-309. This shows that the proposed AwPCSD algorithm performs relatively similar, if not better than the other 3 existing algorithms with less critical parameter to tune.

6. Discussion and conclusion

In this study, the parameter selection of TV-based regularization algorithms is investigated. The sensitivity that the reconstruction image has to value change on each parameter is analysed, in order to know which ones to prioritize when tuning the algorithms to minimize or completely avoid rerunning the reconstruction with different parameters.

In addition, the new adaptive-weighted projection-controlled steepest descent (AwPCSD) algorithm which implements the edge-preserving function for CBCT reconstruction with limited data is proposed. The robustness of new algorithm is tested in comparison with other 3 existing algorithms: ASD-POCS, AwASD-POCS and PCSD. The sensitivity analysis is evaluated experimentally by two image quality metrics: Root mean squared error (RMSE) and Correlation coefficient (CC). The edge preserving property of the adaptive-weighted function is also analysed using the one-dimensional profiles plot along the horizontal and vertical lines of the reconstructed images from the

TV-based algorithms in comparison to the reference image.

The suggested ways of selecting the values for each parameter are presented in detail in the results section. It is clearly seen from the results that parameter choice is crucial for the implementation of TV-based regularization algorithms,especially for the following three parameters: TV hyperparameter (α), Reduction factor of TV hyperparameter (α_{red}) and Maximum ratio of change by TV minimization to change by SART (r_{max}). These parameters are the most sensitive ones and require careful selection of values. Setting these parameters to certain values can significantly deteriorate the quality of final reconstructed image.

With this knowledge, it is a great advantage of PCSD algorithm as well as the proposed AwPCSD algorithm because they do not require the mentioned parameters, making them a lot easier to implement and less prone to errors compared to the ASD-POCS algorithm.

However, the performance of PCSD algorithm is unreliable at times as it performs strangely in response to changes of some parameters such as data-inconsistency-tolerance (ϵ), TV sub-iteration number (ng) and Relaxation parameter (β). In these scenarios, the proposed AwPCSD algorithm shows significant robustness over PCSD algorithm by preserving edges of the reconstructed image better.

The minimization of adaptive-weighted TV norm shows great performance in preserving the edges of the reconstructed algorithms for both two adaptive-weighted algorithms: AwASD-POCS and AwPCSD. This edge-preserving function make the adaptive-weighted algorithms a lot more robust when compared to other two non-adaptive-weighted algorithms, especially for the pair of PCSD and AwPCSD algorithms.

There are limitations of this work regarding the sensitivity analysis of combination of parameters. For some parameters such as the reduction factor of TV hyperparameter (α_{red}), the gradient-descent step-size for the next iteration will only be reduced by α_{red} when the ratio of change due to TV minimization to change due to SART is greater than r_{max} and the L_2 error of image in the current iteration is greater than ϵ simultaneously. This means that all three parameters can affect the results of sensitivity analysis of α_{red} However, the sensitivity analysis is done by varying values of one parameter at a time as the study of combination of parameters would be complicated to evaluate and is beyond the scope of this work.

The proposed AwPCSD algorithm has shown significant robustness compared to other three existing algorithms: ASD-POCS, AwASD-POCS and PCSD. This AwPCSD algorithm is able to preserve the edges of the reconstructed images better with less sensitive parameters to tune. This algorithm will be made available as part of the existing algorithms in TIGRE toolbox.

References

[1] C. Shaw, ed. *Cone Beam Computed Tomography*. Florida: CRC Press, 2014.

[2] A. C. Kak, M. Slaney. *Principles of Computerized Tomographic Imaging*. New York: IEEE Press, 1999.

[3] D.J. Brenner, E.J. Hall. Computed Tomography :An Increasing Source of Radiation Exposure, *The New England Journal of Medicine*, 2007, 357(22), 2277-2284.

[4] A. J. Einstein, M. J. Henzlova, S. Rajagopalan. Estimating Risk of Cancer Associated With Radiation Exposure From 64-Slice Computed Tomography Coronary Angiography. *Journal of the American Medical Association*, 2007, 298, 317-323.

[5] E. Y. Sidky, C. M. Kao, X.Pan. Accurate image reconstruction from few-views and limited-angle data in divergent-beam CT. *Journal of X-Ray Science and Technology*, 2006, 14, 119-139.

[6] G. Chen, J. Tang, S. Leng. Prior image constrained compressed sensing (PICCS)). *Proc. Soc. Photon. Instrum. Eng.*, 2008, 6856 , 1-18.

[7] K. Sauer , B. Liu. Nonstationary filtering of transmission tomograms in high photon counting noise. *IEEE Transactions on Medical Imaging*, 1991, 10(3), 445-452.

[8] L. A. Feldkamp, L. C. Davis, J. W. Kress. Practical cone-beam algorithm. *J.Opt.Soc.Am.*, 1984, A 1, 612-619.

[9] X. Pan, E. Y. Sidky, M. Vannier. Why do commercial CT scanners still employ traditional, filtered back-projection for image reconstruction?. *Inverse Problems*, 2009 , 25(12):123009.

[10] Z. Tian, X. Jia, K. Yuan, T. Pan, S. B. Jiang. Low-dose CT reconstruction via edge preserving total variation regularization. *Physics in Medicine and Biology*, 2011, 56, 5949-5967.

[11] A. J. Jerri. The Shannon Sampling Theorem - Its Various Extensions and Applications : A Tutorial Review. *Proceedings of IEEE*, 1977, 65(11), 1565-1596.

[12] E. Y. Sidky , X. Pan . Image reconstruction in circular cone-beam computed tomography by constrained, total-variation minimization. *Physics in Medicine and Biology*, 2008, 53, 4777-4807.

[13] S. B. Coban, P. J. Withers, W. R. B. Lionheart , S. A. McDonald. When do the iterative reconstruction methods become worth the effort?. 13th International Meeting on Fully Three Dimensional Image Reconstruction in Radiology and Nuclear Medicine (Fully3D 2015), 31 May - 04 June 2015, Newport, Rhode Island, USA 2015.

[14] F. Pontana, J. Pagniez, T. Flohr, J. Faivre, A. Duhamel, J. Remy, M. Remy-Jardin. Chest computed tomography using iterative reconstruction vs filtered back projection (part 1) : evaluation of image noise reduction in 32 patients. *European Radiology*, 2010, 21(3), 627-635.

[15] F. Pontana, J. Pagniez, T. Flohr, J. Faivre, A. Duhamel, J. Remy, M. Remy-Jardin. Chest computed tomography using iterative reconstruction vs filtered back projection (part 2) : image quality of low-dose CT examinations in 80 patients. *European Radiology*, 2010, 21(3), 636-643.

[16] Y. Liu, J. Ma, Y. Fan, Z. Liang. Adaptive-weighted total variation minimization for sparse data toward low-dose x-ray computed tomography image reconstruction. *Physics in Medicine and biology*, 2012, 57, 7923-7956.

[17] X. Lu , Y. Sun , Y. Yuan. Optimization for limited angle tomography in medical image processing. *Pattern Recognition*, 2011, 44(10-11), 2427-2435.

[18] L. Liu, Z. Yin, X. Ma. Nonparametric optimization of constrained total variation for tomography reconstruction. *Computers in Biology and Medicine*, 2013, 43, 2163-2176.

[19] L. Liu, W. Lin, M. Jin. Reconstruction of sparse-view X-ray computed tomography using adaptive iterative algorithms. *Computers in Biology and Medicine*, 2015, 56, 97-106.

[20] W. P. Segars, G. Sturgeon, S. Mendonca, J. Grimes, B. M. W. Tsui. 4D XCAT phantom for multimodality imaging research. *Medical Physics*, 2010, 37 (9), 4902-4915.

[21] A. H. Anderson, A. C. Kak. Simultaneous Algebraic Reconstruction Technique (SART): A superior implementation of the ART algorithm. *Ultrasonic Imaging*, 1984, 6 (1), 81-94.

[22] P. Perona, J. Malik. Scale-space and edge detection using anisotropic diffusion. *IEEE Transactions on Pattern Analysis and Machine Intelligence*, 1990, 12 (7), 629-639.

[23] A. Biguri, M. Dosanjh, S. Hancock, M. Soleimani. TIGRE: a MATLAB-GPU toolbox for CBCT image reconstruction. *Biomedical Physics & Engineering Express*, 2016, 2 (055010).

[24] J. Xu, B. M. W. Tsui. Electronic Noise Modeling in Statistical Iterative Reconstruction. *IEEE Transactions on Image Processing*, 2009, 18(6), 1228-1238.

[25] J. Ma, Z. Liang, Y. Fan, Y. Liu, J. Huang, W. Chen, H. Lu. Variance analysis of x-ray CT sinograms

in the presence of electronic noise background. *Medical Physics*, 2012, 39(7), 4051-4065.

[26] Z. Wang, A.C. Bovik. A Universal Image Quality Index. *IEEE Signal Processing Letters*, 2002, 9 (3), 81-84.

[27] G. Wang, M. Jiang. Ordered-subset simultaneous algebraic reconstruction techniques (OS-SART). *Journal of X-Ray Science and Technology*, 2004, 12, 169-177.

[28] M. Jiang, G. Wang. Convergence Studies on Iterative Algorithms for Image Reconstruction. *IEEE Transactions on Medical Imaging*, 2003, 22(5), 569-579.

[29] P. Perona, J. Malik. Scale-Space and Edge Detection Using Anisotropic Diffusion. *IEEE Transactions on Pattern Analysis and Machine Intelligence*, 1990, 12(7), 629-639.

[30] J. Wang, T. Li, Z. Liang, L. Xing. Dose reduction for kilovotage cone-beam computed tomography in radiation therapy. *Physics in Medicine and Biology*, 2008, 53, 2897-2909.

[31] S.B. Coban and S.A. McDonald. SophiaBeads Datasets. Mar. 2015. DOI: 10.5281/zenodo.16474. URL: http://dx.doi.org/10.5281/zenodo.16474.

[32] S.B. Coban. SophiaBeads Datasets Project Codes. Apr. 2015. DOI: 10.5281/zenodo.16539. URL: http://dx.doi.org/10.5281/zenodo.16539.